Bulletin of the Mineral Research and Exploration

http://bulletin.mta.gov.tr

Comparison of different approaches of computing the tilt angle of the total horizontal gradient and tilt angle of the analytic signal amplitude for detecting source edges

Luan Thanh PHAM[a*], Erdinç ÖKSÜM[b], Thanh Duc DO[a] and Minh Duc VU[a]

[a]*Vietnam National University,University of Science, Faculty of Physics, Department of Geophysics, Hanoi, Vietnam*
[b]*Süleyman Demirel University, Engineering Faculty, Department of Geophysical Engineering, 32200, Isparta, Turkey*

Research Article

Keywords:
Edge Detection, Horizontal Gradient, Analytic Signal, Tilt Angle, Direct Expression, Frequency Technique.

Received Date: 14.04.2020
Accepted Date: 02.06.2020

ABSTRACT

This paper compares effectiveness of the different approaches of computing the tilt angle of the horizontal gradient amplitude and tilt angle of the analytic signal amplitude such as use of direct expression and frequency domain technique (also called k - function) in terms of their accuracy on the detection of the edges of magnetic and gravity sources. These approaches were performed on both synthetic magnetic and gravity data where the frequency domain technique shows improvements in delineation of the actual edges of the sources compared to the direct expression. Additionally, real magnetic data from Zhurihe (Northeast China), and real gravity data from Tuan Giao (Northwest Vietnam) was considered and the obtained results from applying the different approaches were compared with known geological structures. The results show that the boundaries detected from the use of the frequency domain technique are in accord with the known geological structures.

1. Introduction

The knowledge of the edges of the potential field sources is important for geological interpretation because it could delineate subsurface geological structures such as contacts and faults. Many filters have been developed over the decades to detect the source edges, most of which is based on the computation of vertical or horizontal gradients of the field. Evjen (1936), Cordell and Grauch (1985), Roest et al. (1992), Hsu et al. (1996), Fedi and Florio (2001), Fedi (2002), Cella et al. (2009), and Beiki (2010) provided examples of the use of amplitude-based filters to delineate the source edges. The disadvantage of these filters is that they cannot balance the amplitudes of anomalies generated by the sources located at different depths (Ma et al., 2014; Pham et al., 2018*a*, *b*). Several authors developed phase - based methods to highlight the source horizontal boundaries (Miller and Singh, 1994; Rajagopalan and Milligan, 1995; Wijns et al., 2005; Cooper and Cowan, 2006; Cooper and Cowan, 2008; Li et al., 2012; Ma and Li, 2012). The major advantage of these filters is that they make it possible to equalize anomalies from shallow and deep source bodies (Oruç, 2011; Eldosouky, 2019; Pham et al., 2019*a*). However, the universal disadvantages of these filters are that they bring false edges in the output result or the obtained results depend on the window size used. To solve this problem, Ferreira et al. (2013) suggested using a modified version of the tilt angle, called the tilt angle of the horizontal gradient amplitude. Another modified version of the tilt angle, was also introduced by Cooper (2014*a*),

Citation Info: Pham, L. T., Öksüm, E., Do T. D., Vu, M. D. 2021. Comparison of different approaches of computing the tilt angle of the total horizontal gradient and tilt angle of the analytic signal amplitude for detecting source edges. Bulletin of the Mineral Research and Exploration 165, 53-62.
https://doi.org/10.19111/bulletinofmre.746858

**Corresponding author: Luan Thanh PHAM, luanpt@hus.edu.vn*

called the tilt angle of the amplitude of the analytic signal. Both the TTHG and TAS filters are based on the vertical derivative of the nonharmonic functions (the horizontal gradient amplitude THG and the analytic signal amplitude AS). Florio et al. (2006) showed that the vertical derivative of the analytic signal amplitude calculated from the frequency domain technique can be used to estimate the source depth, but it is not effective in detecting the structural index. Ferreira et al. (2013), Yao et al. (2015), Pham et al. (2019*a*) estimated horizontal boundaries by using the vertical derivative of the horizontal gradient amplitude calculated from the frequency domain technique. Cooper (2014*b*), Pham et al. (2019*b*) used a direct expression for computing the vertical derivative of the analytic signal amplitude. Yan et al. (2016) suggested using the frequency domain technique for computing the vertical derivative of the analytic signal amplitude.

In this paper, we compare the edge detection results of the tilt angle of the horizontal gradient amplitude and the tilt angle of the analytic signal amplitude by using the direct expression and the frequency domain technique. The efficacy of the approaches is tested on both synthetic and real magnetic and gravity data.

2. Methods

The tilt angle of the horizontal gradient amplitude is given by (Ferreira et al., 2013)

$$TTHG = tg^{-1}\frac{\frac{\partial THG}{\partial z}}{\sqrt{\left(\frac{\partial THG}{\partial x}\right)^2+\left(\frac{\partial THG}{\partial y}\right)^2}}, \quad (1)$$

where THG is the horizontal gradient amplitude of the filed F, which is given by

$$THG = \sqrt{\left(\frac{\partial F}{\partial x}\right)^2+\left(\frac{\partial F}{\partial y}\right)^2}. \quad (2)$$

The tilt angle of the amplitude of the analytic signal is calculated using the following equation (Cooper, 2014*a*):

$$TAS = tg^{-1}\frac{\frac{\partial AS}{\partial z}}{\sqrt{\left(\frac{\partial AS}{\partial x}\right)^2+\left(\frac{\partial AS}{\partial y}\right)^2}}, \quad (3)$$

where AS is the analytic signal amplitude of the filed F, and is given by

$$AS = \sqrt{\left(\frac{\partial F}{\partial x}\right)^2+\left(\frac{\partial F}{\partial y}\right)^2+\left(\frac{\partial F}{\partial z}\right)^2}. \quad (4)$$

The vertical derivatives of the horizontal gradient amplitude and the analytic signal amplitude can be easily estimated using the direct expressions (Cooper, 2014*b*), as follows:

$$\frac{\partial THG}{\partial z} = \frac{\frac{\partial F}{\partial x}\frac{\partial^2 F}{\partial x \partial z}+\frac{\partial F}{\partial y}\frac{\partial^2 F}{\partial y \partial z}}{THG} \quad (5)$$

and

$$\frac{\partial AS}{\partial z} = \frac{\frac{\partial F}{\partial x}\frac{\partial^2 F}{\partial x \partial z}+\frac{\partial F}{\partial y}\frac{\partial^2 F}{\partial y \partial z}+\frac{\partial F}{\partial z}\frac{\partial^2 F}{\partial z^2}}{AS} \quad (6)$$

Another approach, based on the vertical derivative operator in frequency domain, also can be used to compute the vertical derivative of the horizontal gradient amplitude and the analytic signal amplitude. The definition of the vertical derivative operator is given by Blakely (1995) as follows:

$$\begin{aligned} F\left[\frac{\partial \phi}{\partial z}\right] &= \lim_{\Delta z \to 0}\frac{F[\phi]-F[\phi]e^{-|k|\Delta z}}{\Delta z} \\ &= \lim_{\Delta z \to 0}\frac{1-e^{-|k|\Delta z}}{\Delta z}F[\phi] \\ &= |k|\,F[\phi] \end{aligned} \quad (7)$$

where F[ ] denotes Fourier transformation, ϕ is the horizontal gradient amplitude or the analytic signal amplitude, e is the exponential function and k is the wavenumber defined as

$$k = \sqrt{k_x^2+k_y^2} \quad (8)$$

where k_x and k_y are the wavenumbers in the x and y directions, respectively. The inverse Fourier transform of Equation (7) provides the vertical derivative of the function ϕ. Note that the horizontal derivatives in Equation (1) and (3) are computed in the space domain using the finite difference method.

3. Theoretical Examples

In this section, we compare the edge detection results of the TTHG and TAS by using the direct expressions with the results obtained by using the frequency domain approach. The first model considered includes three magnetized prisms located at different depths. Figure 1a shows the 3D perspective view of the model. The prismatic sources have the same size of 30×130×5 km. The top of the sources 1A, 1B, and

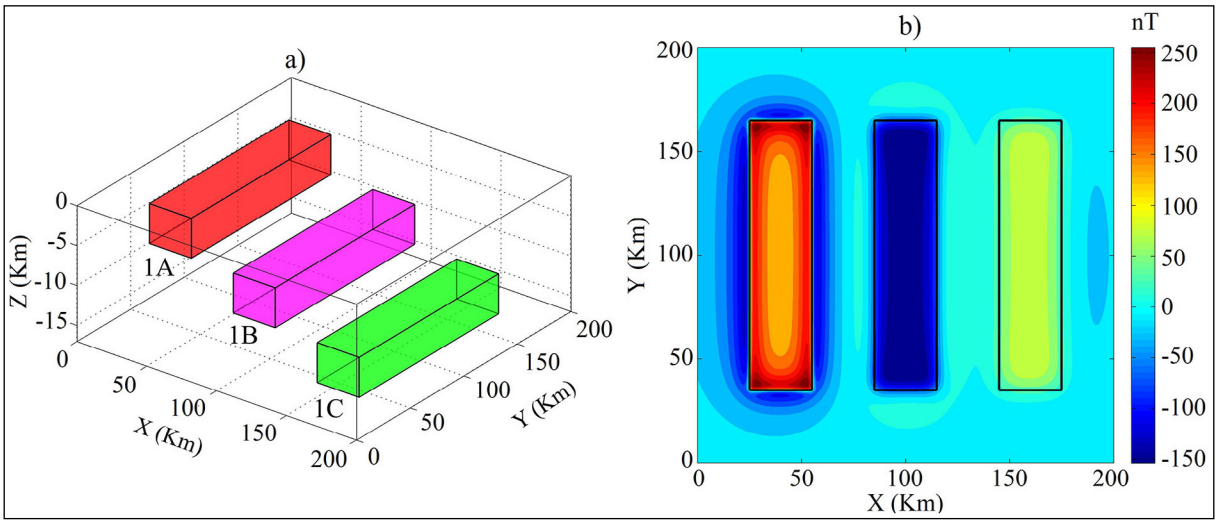

Figure 1- a) Perspective view of the first model, consisting of three magnetic sources (1A, 1B and 1C) with top depths of 1 km, 6 km and 11 km, respectively, b) synthetic magnetic field generated by the model. The black lines show actual edges of the sources.

1C are 1, 6, and 11 km, respectively. The sources have a magnetic declination of 0° and an inclination of 90°. The magnetization magnitudes of the sources 1A, 1B, and 1C are 1, -1.2, and 1 A/m, respectively. We computed the magnetic anomaly produced by these three prismatic sources on a grid of 201×201 points with 1 km spacing. The magnetic anomaly of the model is shown in Figure 1b. Figure 2a shows TTHG result obtained from using the direct expression. As can be seen from this figure, although the use of the direct expression can detect all the source edges, it brings spurious maxima around the prismatic bodies. In addition, this approach also generates maximum values over the sources. Figure 2b shows the TTHG result obtained from using the frequency domain vertical derivative operator. We can see that, in this case, the TTHG cannot only highlight all the source horizontal boundaries, but also can avoid generating spurious boundaries. Figure 2c shows TAS result obtained from using the direct expression. As depicted in this figure, the use of the direct expression can highlight the source horizontal boundaries. However, this approach brings spurious maxima between the sources. Figure 2d shows TAS result obtained from using the frequency domain vertical derivative operator. Clearly, in this case, the TAS can detect all the source edges without any spurious edges.

Since the very complex nature of the geological phenomena, it is necessary to also test the performance of these approaches in a more complex model. Here, we consider a gravity model that includes six prismatic sources. Figure 3a shows the 3D perspective view of the model. The geometric and density parameters are presented in Table 1. The gravity anomaly due to the model is computed on a grid of 201×201 points with 1 km spacing, and is shown in Figure 3b. Figure 4a shows the TTHG result obtained from using the direct expression. As clearly seen from this figure, the TTHG filter can highlight the source horizontal boundaries, but it produces some of the artefacts over source 2C and between sources 2A and 2D. Figure 4b depicts TTHG result by using the frequency domain approach. We can see that, in this case, the TTHG is effective in detecting all the source horizontal boundaries without any other spurious boundaries. Figure 4c and d depict TAS results obtained from using the direct expression and the frequency domain approach, respectively. For both forms of the calculations, the TAS filter cannot highlight the edges of the thin sources (2D and 2E). Moreover, the use of the direct expression also produces a spurious boundary between sources 2A and 2D, and spurious minimum contours around the source 2B and between sources 2D and 2E.

To further test the stability of the approaches, the data in Figure 3b was corrupted with random noise with amplitude equal to 5% of the anomaly amplitude. Figure 5a shows noise - corrupted gravity data. Because the TTHG and TAS filters use second-order derivatives of the field, they are sensitive to noise. To attenuate the noise effect, an upward continuation of 2 km was applied to the noise data prior to calculating the filters. Figure 5b shows the transformed field after

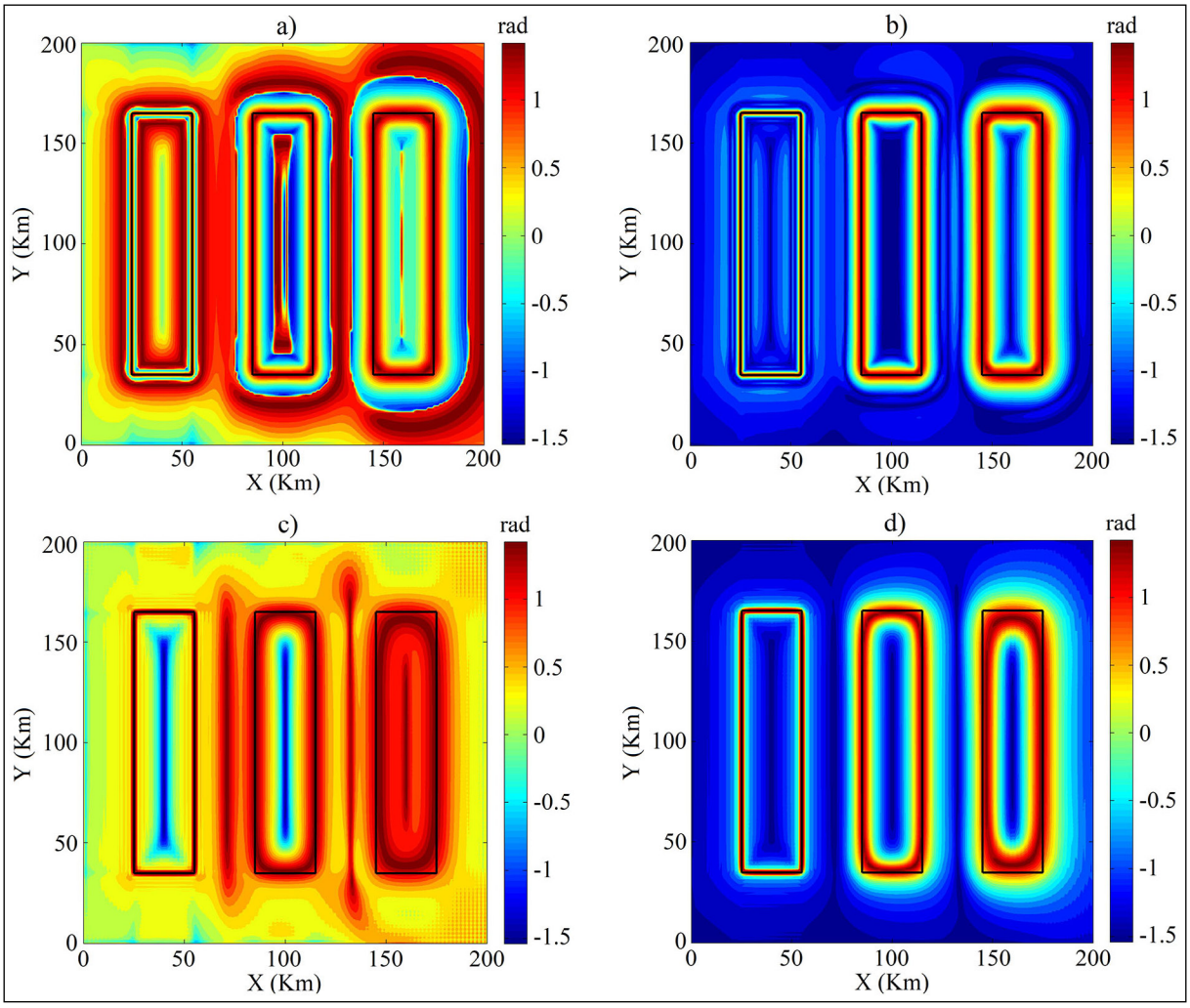

Figure 2- a) TTHG using the direct expression, b) TTHG using the frequency domain approach, c) TAS using the direct expression, d) TAS using the frequency domain. The black lines show actual edges of the sources.

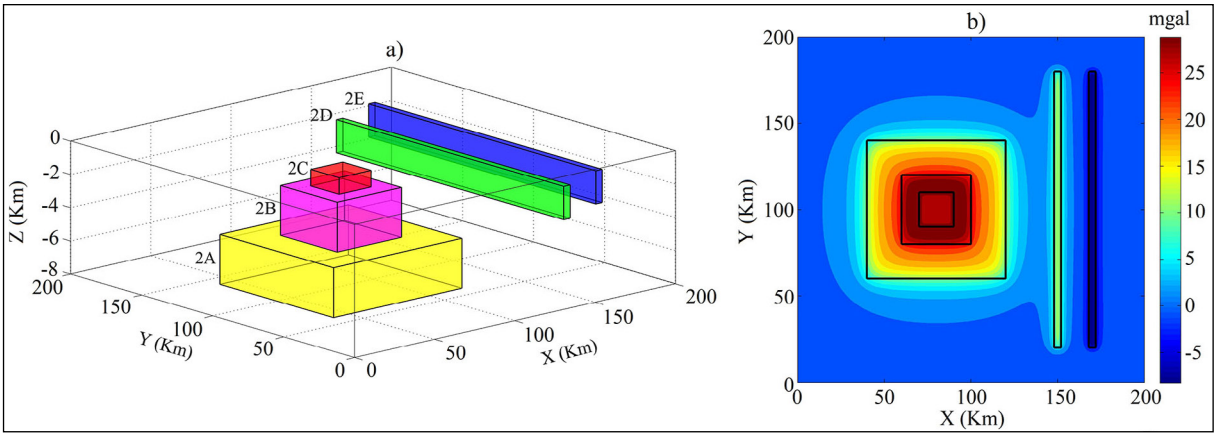

Figure 3- a) Perspective view of the second model; b) synthetic gravity field generated by the model. The black lines show actual edges of the sources.

Table 1- The geometric and density parameters of the second model.

Parameters / Prism ID	2A	2B	2C	2D	2E
x-coordinates of center (km)	80	80	90	150	170
y-coordinates of center (km)	100	100	100	100	100
Width (km)	20	40	80	4	4
Length (km)	20	40	80	160	160
Depth of top (km)	1	2	5	1.5	1
Depth of bottom (km)	2	5	8	3.5	3
Density contrast (g/cm^3)	-0.1	0.1	0.2	0.3	-0.2

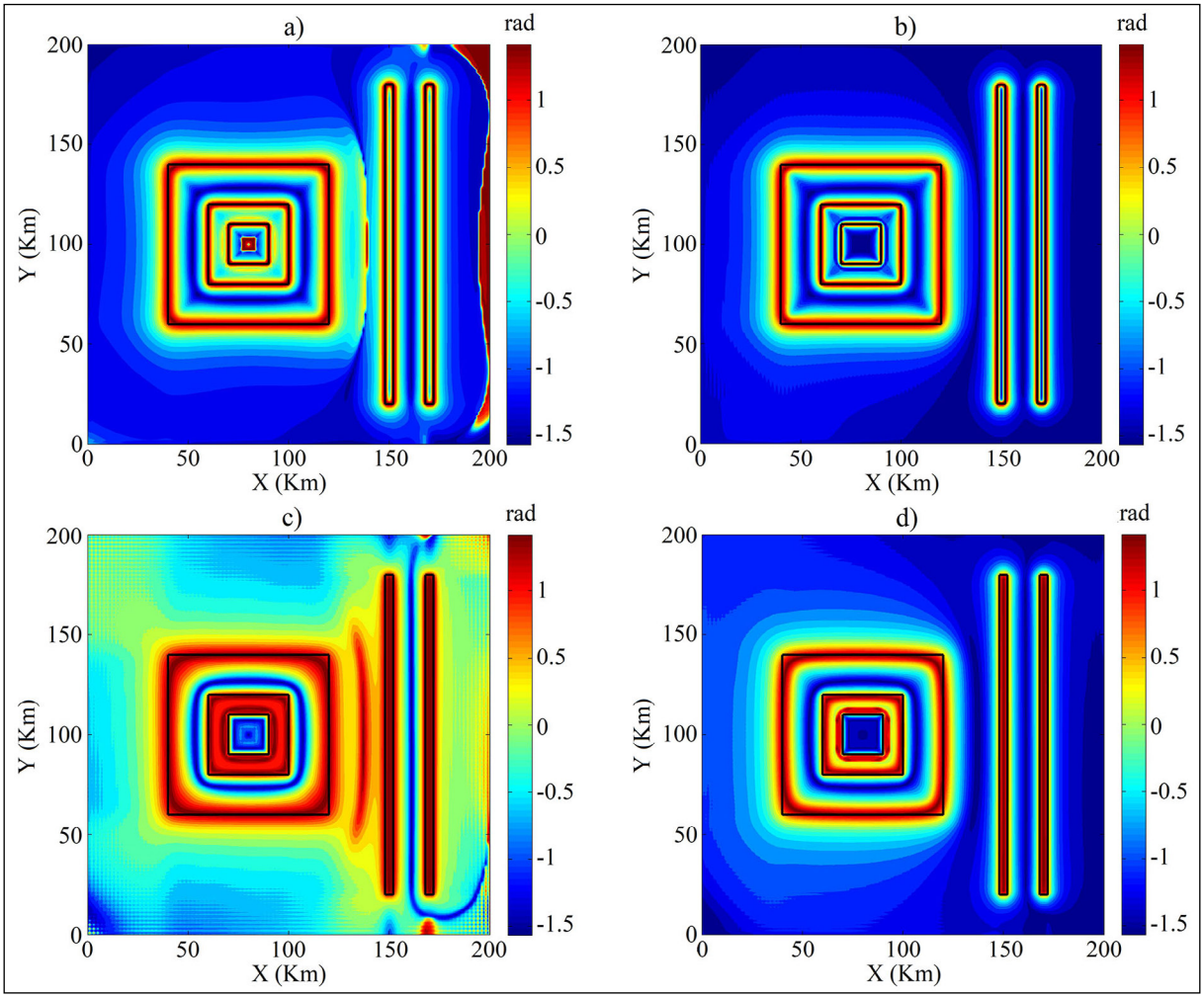

Figure 4- a) TTHG using the direct expression, b) TTHG using the frequency domain approach, c) TAS using the direct expression, d) TAS using the frequency domain. The black lines show actual edges of the sources.

the upward continuation where the effect of the high frequency noise was attenuated somewhat. Figure 6a and b display TTHG results obtained from performing the direct expression and the frequency domain approach, respectively. Clearly, both the approaches can delineate all the source edges, but the use of the direct expression brings some false maxima over the source 2C. Figure 6c and d displays TAS results obtained from using the direct expression and the frequency domain approach, respectively. It can be clearly seen that the edges of the thin sources (2D and 2E) could not be outlined by the TAS filter, and

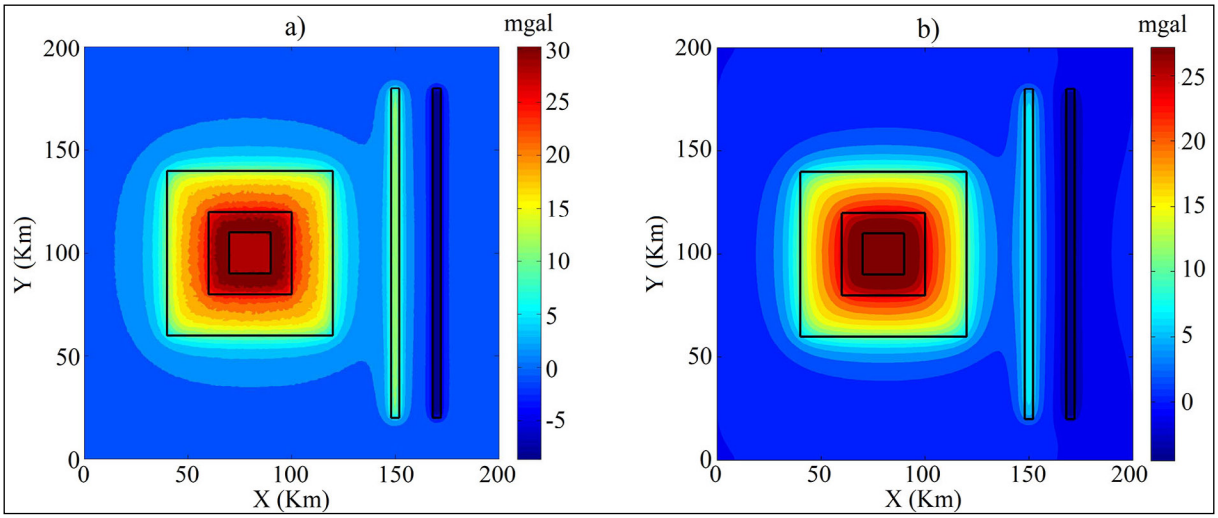

Figure 5- a) Synthetic gravity field generated by the second model with 5% random noise, b) synthetic gravity field after upward continuation of 2 km. The black lines show actual edges of the sources.

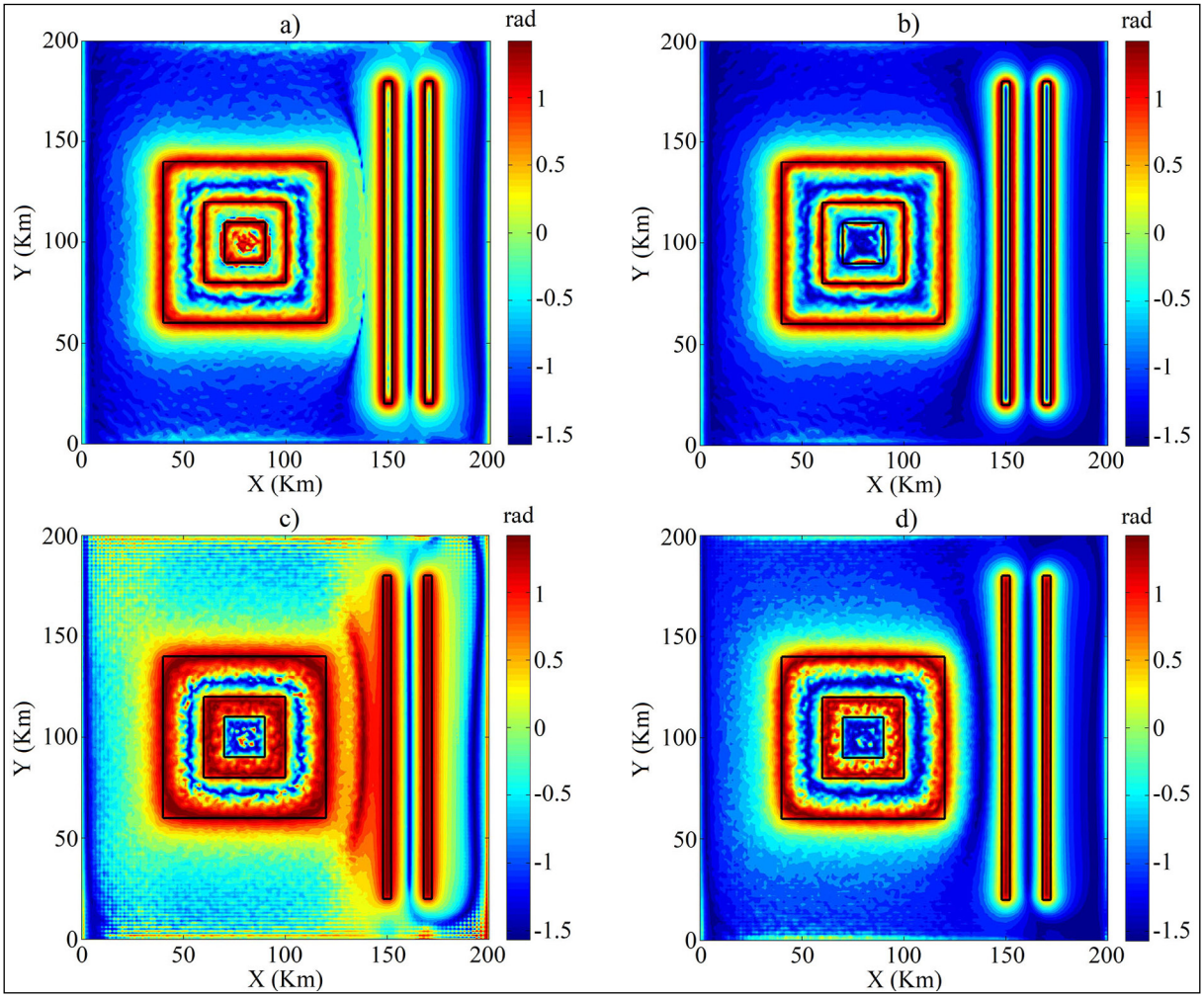

Figure 6- a) TTHG using the direct expression, b) TTHG using the frequency domain approach, c) TAS using the direct expression, d) TAS using the frequency domain. The black lines show actual edges of the sources.

the use of the direct expression produces a spurious edge between sources 2A and 2D. Moreover, the TAS is more sensitive to noise than the TTHG as it uses second-order vertical derivative of the field, whereas the TTHG uses only the first-order vertical derivative.

4. Application to Real Data

In order to test the practical applicability of the approaches, we apply them to real magnetic data from Zhurihe (Northeast China), and real gravity data from Tuan Giao (northwest Vietnam).

Figure 7a shows the magnetic anomaly data reduced to the pole of the Zhurihe area (Yuan and Yu, 2014). The study area is 73×117 km, with an interval of 1 km along the east and north directions. Figure 7b and c show TTHG results obtained from using the direct expression and frequency domain approach, respectively. Figure 7d and e show TAS maps obtained from the use of the direct expression and frequency domain approach, respectively. Figure 7f displays geological map of the area (modified from Ma et al., 2014). The continental sediments cover most of the Zhurihe area, except for some nearly SE - NW trending iron-rich sandstone dykes (Ma et al., 2014, Zhou et al., 2017). As can be observed, the edge maps of the TTHG are consistent with the geology information (Figure 7f). In this case, the TAS is less effective in highlight the geological boundaries, and it is more sensitive to noise than the TTHG. However, it

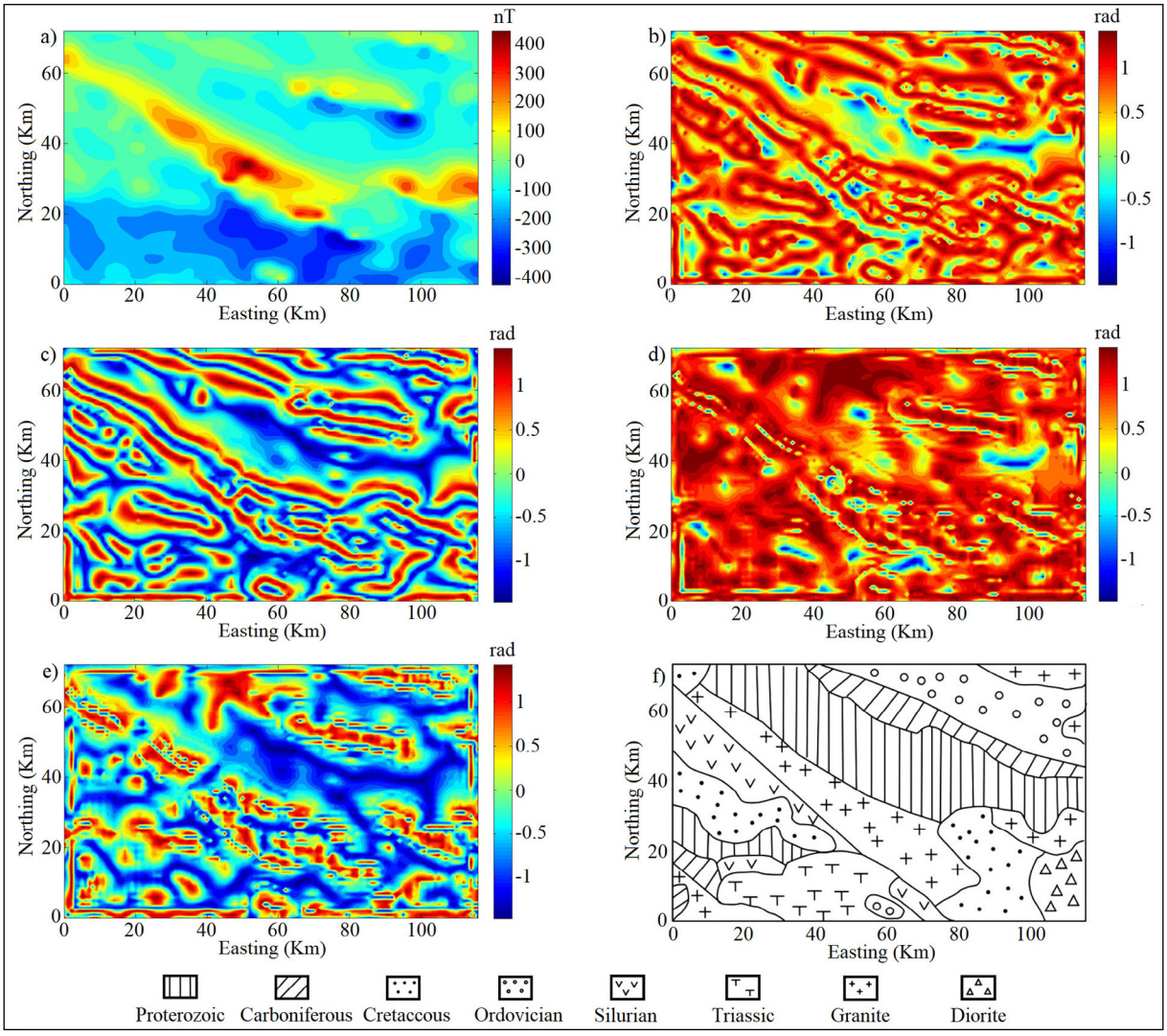

Figure 7- a) Magnetic anomaly data reduced to the pole of the Zhurihe area, b) TTHG using the direct expression, c) TTHG using the frequency domain approach, d) TAS using the direct expression, e) TAS using the frequency domain, f) geological map of the area (Ma et al., 2014).

is worth noting that the use of the frequency domain approach for both the TTHG and TAS filters provides more clearly results, compared to the use of the direct expression.

Figure 8a shows the Bouguer gravity anomaly map of the Tuan Giao area (Pham et al., 2019*a*). The study area is characterized by high seismicity (Roger et al., 2014; Duan and Duong, 2017), covering an area about 116 km × 155 km with an interval of 1.22 km along the east and north directions. Figure 8b and c display TTHG maps obtained from the use of the direct expression and frequency domain approach, respectively. Figure 8d and e display TAS results obtained from using the direct expression and frequency domain approach, respectively. Figure 8f displays geological map of the area (modified from Roger et al., 2012). The Tuan Giao area has complex SE-NW trending geological structures including many faults, sedimentary rocks, magmatic rocks, and volcanoes. We can see that, the horizontal boundaries detected by the TTHG are consistent with the geology information (Figure 8f). In addition, the use of the frequency domain approach for calculating the TTHG shows a more clearly result compared to the use of the direct expression. The TAS results by both approaches are less effective in detecting the geological boundaries compared to those obtained from the TTHG filter. However, similar to the TTHG case, the use of the frequency domain approach for calculating the TAS brings a more clearly result compared to the use of the direct expression.

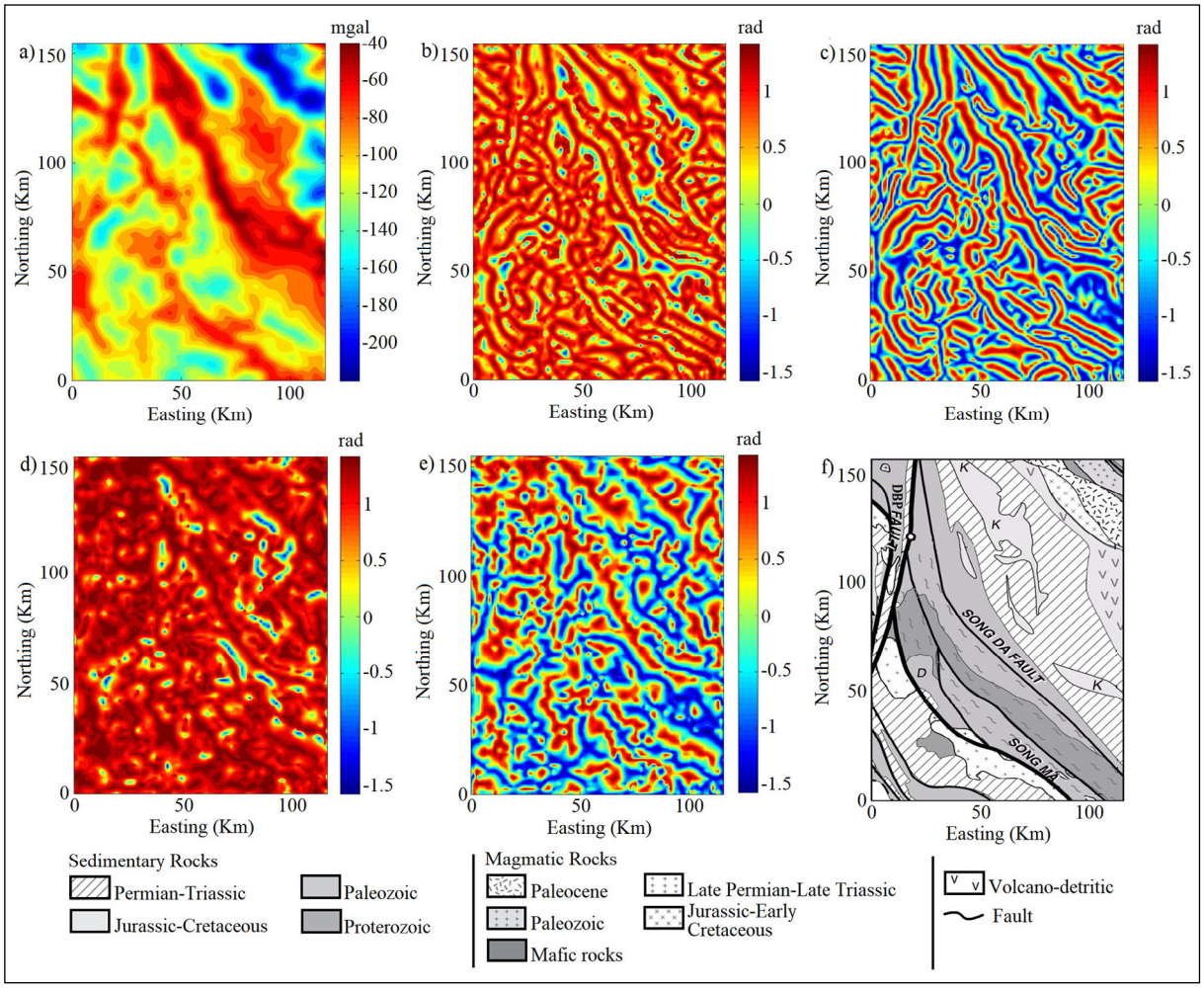

Figure 8- a) Bouguer gravity anomaly of the Tuan Giao area, b) TTHG using the direct expression, c) TTHG using the frequency domain approach, d) TAS using the direct expression, e) TAS using the frequency domain, f) geological map of the area (Roger et al., 2012).

5. Results

We tried to review the effectiveness of the use of the frequency domain approach and direct expression to compute the tilt angle of the total horizontal gradient and tilt angle of the analytic signal amplitude for detecting the source edges. Test studies were performed on a synthetic magnetic data, and also on synthetic gravity data with and without random noise. The obtained results showed that the use of the frequency domain approach is more effective in highlighting the geological boundaries compared to the use of the direct expression. Test studies also were performed on real magnetic data of the Zhurihe area (Northeast China), and real gravity data of the Tuan Giao area (northwest Vietnam), where edges obtained from using the frequency domain approach are in accord with the known geological structures. We also showed that the edges detected from the tilt angle of the total horizontal gradient are more clearly than those from the tilt angle of the analytic signal amplitude.

Acknowledgement

The authors record with pleasure their sincere thanks to the editor and the reviewers for their very constructive suggestions to improve the paper. This research is funded by the Vietnam National University, Hanoi (VNU) under project number QG.20.13.

References

Beiki, M. 2010. Analytic signals of gravity gradient tensor and their application to estimate source location. Geophysics 75 (6), 159-174.

Blakely, R. J. 1995. Potential Theory in Gravity and Magnetic Applications. Cambridge. Cambridge University Press, Cambridge, 326.

Cella, F., Fedi, M., Florio, G. 2009. Toward a full multiscale approach to interpret potential fields. Geophysical Prospecting 57, 543-557.

Cooper, G. R. J. 2014*a*. Reducing the dependence of the analytic signal amplitude of aeromagnetic data on the source vector direction. Geophysics 79, J55-J60.

Cooper, G. R. J. 2014*b*. The automatic determination of the location and depth of contacts and dykes from aeromagnetic data. Pure and Applied Geophysics 171(9), 2417-2423.

Cooper, G. R. J., Cowan, D. R. 2006. Enhancing potential field data using filters based on the local phase. Computers and Geosciences 32, 1585-1591.

Cooper, G. R. J., Cowan, D. R. 2008. Edge enhancement of potential - field data using normalized statistics. Geophysics 73(3), H1-H4.

Cordell, L., Grauch, V. J. S. 1985. Mapping basement magnetization zones from aeromagnetic data in the San Juan Basin, New Mexico, in Hinze, William J. (Ed.), The utility of regional gravity and magnetic anomaly maps: Society of Exploration Geophysicists, Tulsa, Oklahoma, 1985, 181-197.

Duan, B. V., Duong, N. A. 2017. The relation between fault movement potential and seismic activity of major faults in Northwestern Vietnam. Vietnam Journal of Earth Sciences 39(3), 240-255.

Eldosouky, A. M. 2019. Aeromagnetic data for mapping geologic contacts at Samr El-Qaa area, North Eastern Desert, Egypt. Arabian Journal of Geosciences 12, 2.

Evjen, H. M. 1936. The place of the vertical gradient in gravitational interpretations. Geophysics 1(1), 127-136.

Fedi, M. 2002. Multiscale derivative analysis: A new tool to enhance detection of gravity source boundaries at various scales. Geophysical Research Letters 29(2), 1029.

Fedi, M., Florio, G. 2001. Detection of potential fields source boundaries by enhanced horizontal derivative method. Geophysical Prospecting 49(1), 40-58.

Ferreira, F. J. F., de Souza, J., de Bongiolo, A. B. E. S., de Castro, L. G. 2013. Enhancement of the total horizontal gradient of magnetic anomalies using the tilt angle. Geophysics 78(3), J33-J41.

Florio, G., Fedi, M., Pastek, R. 2006. On the application of Euler deconvolution to the analytic signal. Geophysics 71(6), L87-L93.

Hsu, S. K., Coppense, D., Shyu, C. T. 1996. High - resolution detection of geologic boundaries from potential field anomalies: An enhanced analytic signal technique. Geophysics 61, 1947-1957.

Li, L., Ma, G., Du, X. 2012. Edge Detection in Potential-Field Data by Enhanced Mathematical Morphology Filter. Pure and Applied Geophysics 170(4), 645-653.

Ma, G., Li, L. 2012. Edge detection in potential fields with the normalized total horizontal derivative. Computers and Geosciences 41, 83-87.

Ma. G., Liu, C., Li, L. 2014. Balanced horizontal derivative of potential field data to recognize the edges and estimate location parameters of the source. Journal of Applied Geophysics 108, 12-18.

Miller, H. G., Singh, V. 1994. Potential field tilt a new concept for location of potential field sources. Journal of Applied Geophysics 32, 213-217.

Oruç, B. 2011. Edge detection and depth estimation using a tilt angle map from gravity gradient data of the Kozaklı - Central Anatolian Region, Turkey. Pure and Applied Geophysics 168, 1769-1780.

Pham, L.T., Oksum, E., Do, T. D., Le - Huy, M. 2018*a*. New method for edges detection of magnetic sources using logistic function. Geofizichesky Zhurnal 40(6), 127-135.

Pham L. T., Le-Huy M., Oksum, E., Do T. D. 2018*b*. Determination of maximum tilt angle from analytic signal amplitude of magnetic data by the curvature - based method. Vietnam Journal of Earth Sciences 40(4), 354-366.

Pham, L. T., Oksum, E., Do, T. D. 2019*a*. Edge enhancement of potential field data using the logistic function and the total horizontal gradient. Acta Geodaetica et Geophysica 54, 143-155.

Pham, L. T., Oksum, E., Do, T. D., Le - Huy, M., Vu, M. D., Nguyen, V.D. 2019*b*. LAS: a combination of the analytic signal amplitude and the generalised logistic function as a novel edge enhancement of magnetic data. Contributions to Geophysics and Geodesy 49(4), 425-440.

Rajagopalan, S., Milligan, P. 1995. Image enhancement of aeromagnetic data using automatic gain control. Exploration Geophysics 25, 173-178.

Roest, W. R. J., Verhoef, J, Pilkington, M. 1992. Magnetic interpretation using the 3-D analytic signal. Geophysics 57(1), 116-125.

Roger, F., Maluski, H., Lepvrier, C., Tich, V. V., Paquette, J. L. 2012. LA - ICPMS zircons U / Pb dating of Permo - Triassic and Cretaceous magmatisms in Northern Vietnam - geodynamical implications. Journal of Asian Earth Sciences 48, 72-82.

Roger, F., Jolivet, M., Maluski, H., Respaut, J. P., Münch, P., Paquette, J. L., Vu - Van, T., Vu - Van, V. 2014. Emplacement and cooling of the Dien Bien Phu granitic complex: implications for the tectonic evolution of the Dien Bien Phu fault (Truong Son Belt, NW Vietnam). Gondwana Research 26(2), 785-801.

Wijns, C., Perez, C., Kowalczyk, P. 2005. Theta map: edge detection in magnetic data. Geophysics 70, 39-43.

Yan, T. J., Wu, Y. G., Yuan, Y., Chen, L. N. 2016. Edge detection of potential field data using an enhanced analytic signal tilt angle. Chinese Journal of Geophysics 59(4), 341-349.

Yao, Y., Huang, D., Yu, X., Chai, B. 2015. Edge interpretation of potential field data with the normalized enhanced analytic signal. Acta Geodaetica et Geophysica 51(1), 125-136.

Yuan, Y., Yu, Q. 2014. Edge detection in potential-field gradient tensor data by use of improved horizontal analytical signal methods. Pure and Applied Geophysics 172(2), 461-472.

Zhou, S., Huang, D., Jiao, J. 2017. Total horizontal derivatives of potential field three - dimensional structure tensor and their application to detect source edges. Acta Geodaetica et Geophysica 52(3), 317-329.